

# Tunable interfacial properties of epitaxial graphene on metal substrates

Min Gao,<sup>1</sup> Yi Pan,<sup>1</sup> Chendong Zhang,<sup>1</sup> Hao Hu,<sup>1</sup> Rong Yang,<sup>1</sup> Hongliang Lu,<sup>1</sup> Jinming Cai,<sup>1</sup> Shixuan Du,<sup>1</sup> Feng Liu,<sup>2</sup> and H.-J. Gao<sup>1,a)</sup>

<sup>1</sup>Institute of Physics, Chinese Academy of Sciences, Beijing 100190, People's Republic of China

<sup>2</sup>Department of Materials Science and Engineering, University of Utah, Salt Lake City, Utah 84112, USA

(Received 22 December 2009; accepted 14 January 2010; published online 3 February 2010)

We report on tuning interfacial properties of epitaxially-grown graphenes with different kinds of metal substrates based on scanning tunneling microscopy experiments and density functional theory calculations. Three kinds of metal substrates, Ni(111), Pt(111), and Ru(0001), show different interactions with the epitaxially grown graphene at the interfaces. The different interfacial interaction making graphene *n*-type and *p*-type doped, leads to the polarity change of the thermoelectric property of the graphene/metal systems. These findings may give further insights to the interfacial interactions in the graphene/metal systems and promote the use of graphene-based heterostructures in devices. © 2010 American Institute of Physics. [doi:10.1063/1.3309671]

Graphene, a truly two-dimensional (2D) zero-gap semiconductor, has attracted much recent attention due to its peculiar properties and potential applications.<sup>1–8</sup> To conduct graphene measurements (such as transport measurements) as well as to realize the potential applications of graphene, it is often required to have graphene supported on a substrate, either directly growing graphene on a substrate<sup>9–13</sup> or transferring it onto a foreign substrate.<sup>1–3,5,6,8,14</sup> However, most existing investigations have focused on the in-plane characteristics of single layer graphene, while much less is known for the interfacial properties between graphene and substrate. The interfacial interaction may not only affect the in-plane properties of 2D freestanding graphene<sup>15</sup> but also play a critical role in graphene-based heterostructures that can be used as device building blocks. Therefore, it is highly desirable to understand how graphene interacts with the underlying substrates, and better yet to control their interfacial and thus the physical properties of the graphene-based systems.

In this letter, we demonstrate the possibility of tuning the interfacial properties between graphene and different kinds of metal substrates. Using epitaxial growth of graphene on Ni(111), Ru(0001), and Pt(111) as model systems, we performed a comparative study that reveals an interesting dependence of interfacial interaction and thermoelectric potential properties. Scanning tunneling microscopy (STM) results show different amounts of surface corrugation due to the different strength of interfacial interaction, which is reflected by the average “bond” length between graphene overlayer and substrates from our first-principles density functional theory (DFT) calculations. The different interfacial interaction leads to the change of the thermoelectric property.

Our experiment was conducted in an ultra high vacuum (UHV) chamber with the base pressure lower than  $1 \times 10^{-10}$  mbar. The chamber was equipped with an STM, a low energy electron diffraction (LEED), an Auger electron spectroscopy (AES), and an electron beam heating stage. The substrates were commercial products with surface polished to less than  $0.03 \mu\text{m}$  of roughness. They were cleaned by several cycles of ultrasonic cleaning in acetone and ethanol to remove organic contaminants on the surface. Then the

crystal was loaded into the UHV chamber and cleaned using cycles of 0.6 keV Ar<sup>+</sup> sputtering followed by annealing to high temperature. We prepared high quality graphene by thermal decomposition of hydrocarbon, ethylene, on metal substrates at high temperature. The amount of exposure is 100 langmuir, sufficient for the formation of one layer of graphene. Afterwards, we applied AES spectra to analyze the chemical composition of surface. The spectra showed a sharp peak for carbon at 272 eV and no obvious signature for other elements except the substrate, confirming that the carbon element appears on the substrate. The thermoelectric measurements of the heterostructures were conducted using a four-probe STM system in another UHV chamber.

To investigate the interfacial properties, epitaxial graphene was prepared on three kinds of metal substrate, i.e., Ni(111), Ru(0001), and Pt(111). Figures 1(a)–1(c) show STM images of the epitaxially-grown graphene on Ni(111), Ru(0001), and Pt(111), respectively. The inset images in Fig. 1 are the corresponding LEED patterns. In Fig. 1(a), graphene on Ni(111) forms a perfect atomic lattice without surface corrugation (Moiré pattern) and the corresponding LEED pattern [inset of Fig. 1(a)] shows only one set of lattice, indicating carbon atoms in the graphene overlayer bond nicely and strongly one-to-one with the underlying Ni surface atoms. For the graphene on Ru(0001), a single-domain overlayer structure can be still formed but with large surface corrugations (Moiré patterns),<sup>10–12</sup> as it can be seen in the

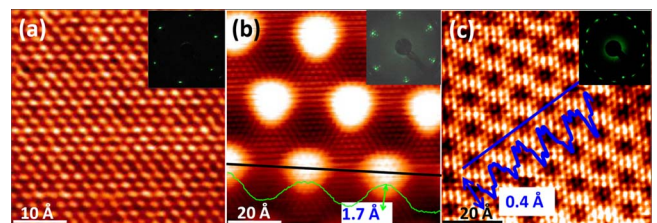


FIG. 1. (Color online) Atomic resolution STM images: (a) graphene on Ni(111) grown at 700 °C, (b) graphene on Ru(0001) grown at 800 °C, (c) graphene on Pt(111) grown at 600 °C. Scan parameter: (a)  $V_S = -40$  mV,  $I = 1.5$  nA, (b)  $V_S = -300$  mV,  $I = 1.3$  nA, and (c)  $V_S = -0.4$  V,  $I = 0.2$  nA. The inset is the corresponding LEED pattern of the sample. The beam energy is 60 eV. The height profile is taken along the line in (b) and (c), showing the corrugation of graphene on Ru(0001) and Pt(111).

<sup>a)</sup>Electronic mail: hjgao@iphy.ac.cn.

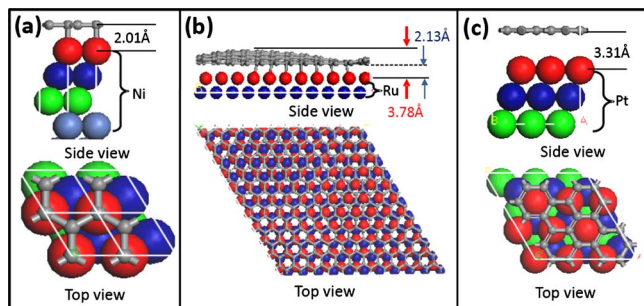


FIG. 2. (Color online) The atomic model of graphene on Ni(111), Pt(111) and Ru(0001). Small atoms are graphene and big atoms are substrate atoms. (a) Graphene on Ni(111). The interfacial distance is 2.01 Å. (b) Graphene on Ru(0001). The distance is 2.13 Å and 3.79 Å. (c) Graphene on Pt(111). The distance is 3.31 Å.

STM image and LEED pattern in Fig. 1(b). The line profile along the black line in Fig. 1(b) shows a large graphene surface corrugation with an average height variation of  $\sim 1.7$  Å. The brightest regions are the “top” highest regions, and the darkest regions are lower at the “bottom.” The LEED pattern of graphene on Pt(111) [inset of Fig. 1(c)] shows fragmented diffraction rings, indicating that there are domains of different orientations of graphene on Pt(111) surface. Figure 1(c) gives the STM image of a  $14^\circ$  rotation domain, showing a  $(4 \times 4)$  superstructure with respect to graphene and a  $(\sqrt{13} \times \sqrt{13})R14^\circ$  superstructure to Pt(111). The line profile in Fig. 1(c) shows that the average height variation is  $\sim 0.4$  Å, much smaller than 1.7 Å in the graphene/Ru(0001) system. There exist other orientations of graphene on Pt, which was discussed before.<sup>16</sup> All the domains have only small height variations.

The relative strength of interfacial interaction in the three experimental systems is further confirmed by DFT calculations of interfacial spacing, i.e., the bonding distance between graphene and metal substrates. For the graphene/Ni(111) (graphene is referred as G in the following) system, we built a one-to-one model as shown in Fig. 2(a). The calculated distance between graphene and Ni(111) is 2.01 Å. For the G/Ru(0001) system, according to the experiment, a 12-to-11 model with a  $(12 \times 12)$  graphene unit cell matched onto a  $(11 \times 11)$  Ru cell was built to calculate. As shown in Fig. 2(b), the graphene is corrugated; the vertical distances from the top region and the bottom region of graphene to Ru(0001) surface are 3.78 and 2.13 Å, respectively. For the G/Pt(111) system, we used a structure model shown in Fig. 2(c), in which graphene lattice is rotated by  $30^\circ$  with respect

to the lattice of Pt(111).<sup>17</sup> The optimized distance between graphene and Pt(111) is 3.31 Å.

The different interfacial interaction strength is expected to influence the electronic and transport properties of graphene overlayer. We measured the interfacial thermoelectric properties of three G/metal heterostructures in our four-probe STM system.<sup>18</sup> In order to keep the original structure of the graphene layer from being destroyed during the measurement, the soft metal indium was used to coat the ordinary tungsten tip. It was made by dipping one of the four tips slightly into melted indium and then approaching to the graphene surface. The measurement setup is shown in Fig. 3(a). The temperature of the tip was kept constant, and the substrate is heated up from 300 to 450 K. The  $I$ - $V$  curve was measured when the tip kept a good contact with substrate. Figure 3(b) shows the  $I$ - $V$  curves of the G/Pt(111) system at different temperatures. The slope of a curve is correlated with the contact resistant between the tip and the sample. Note that all the  $I$ - $V$  curves show an offset voltage when the current is equaled to zero. This offset voltage, originated from the thermoelectric effect, can be equaled to the thermoelectric potential; it increases with the increasing substrate temperature as expected. Thus, for the weakly interactive G/Pt(111) interface, the thermoelectric potential is always positive, meaning that the electron current (opposite of the electric current flow) driven by the temperature difference between the tip and the substrate flows from the tip to the substrate. Figure 3(c) shows a set of measurements for G/Ru(0001) at substrate temperature of 450 K. The most interesting observation is that there are two states of  $I$ - $V$  curves: one with positive thermoelectric potential and the other with negative potential. We make the tip slowly approach the surface. When the tip just touches the surface, we first observed a positive thermoelectric potential [line 1 in Fig. 3(c)]. When the tip is pressed further down to the surface, we then observed a negative potential (line 2). This reversal of polarity of thermoelectric potential can be associated with the fact that the tip is initially in contact with the top graphene region and later with the bottom region when it is pressed down. These observations suggest that the thermoelectric potential varies spatially in G/Ru(0001) surface.

For the G/Ni(111) interface and the pure Pt(111) substrate, the thermoelectric potential is found always negative. Figure 4 shows the measured thermoelectric potentials as a function of temperature in the three systems together with the results of pure Pt substrate. By a linear fitting to the data, the Seebeck coefficients, having the contrary sign to the slope, are extracted to be  $-0.025$ ,  $-0.019$ ,  $0.037$ , and  $0.046$

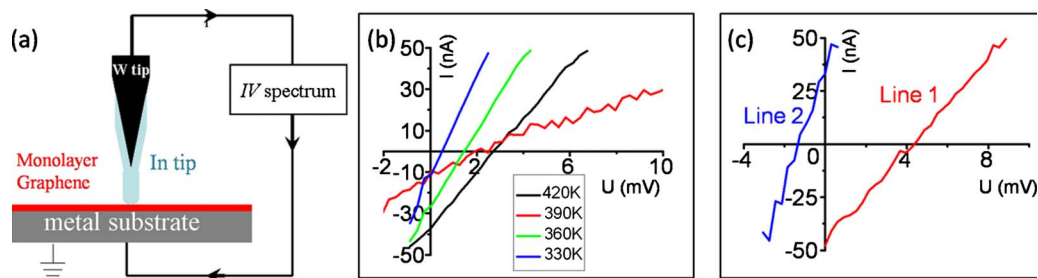


FIG. 3. (Color online) (a) Sketch of thermoelectric measurement. The W tip is coated with indium. (b) The  $I$ - $V$  curve of graphene on Pt(111) at 330, 360, 390, and 420 K. (c) The  $I$ - $V$  curve of graphene on Ru(0001) at 450 K. It has two typical states: positive thermoelectric potential and negative thermoelectric potential. It show the variation from positive state (line 1) to negative state (line 2) when the tip approaches by a step.

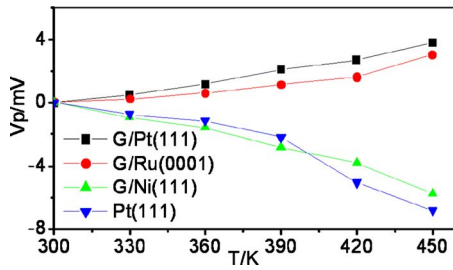


FIG. 4. (Color online) The voltage-temperature ( $V$ - $T$ ) curves of graphene on metal surfaces, in comparison with the  $V$ - $T$  curve of bare Pt(111) surface.

mV/K for G/Pt(111), G/Ru(0001), G/Ni(111), and Pt(111) substrate, respectively. We note that these values are quite different from the predicted in-plane Seebeck coefficient of graphene.<sup>19</sup>

The changes of the interfacial thermoelectric potential can be understood in terms of graphene doping level or change of Fermi energy. The transport properties of the metal/graphene/metal heterostructure for different types of graphene doping were conducted, using the Landauer-Buttiker formula within the framework of single-band tight-binding model.<sup>20</sup> For the G/Ni(111) interface, our DFT calculations show that there is a large amount electron charge transfer from Ni substrate to graphene raising the Fermi level above the Dirac point, so that graphene is effectively  $n$ -type doped like a metal.<sup>21,22</sup> This makes the graphene heterostructure behave similarly to the pure metal junctions with a negative thermoelectrical potential (electrons flow along temperature gradient). For the G/Pt(111) interface, graphene is found to be a  $p$ -type (Fermi level below Dirac point). Consequently, the graphene hetero-structure has a positive thermoelectrical potential. In contrast, on G/Ru(0001), our calculations show that there is a noticeable electron charge transfer from the top to the bottom region, so that the top becomes electron deficient of  $p$ -type while the bottom becomes electron rich of  $n$ -type. Consequently, the doping type varies spatially, which in turn leads to spatially varying polarity of thermoelectric potential, being positive in the top region and negative in the bottom region of graphene, same as the experimental observation presented in supporting information.

In summary, using STM measurements combined with DFT calculations, we show that by using different kinds of metal substrates, the interfacial properties between graphene and metal substrates have been tuned. We have further demonstrated that the interaction between the graphene and the substrates at the interfaces can tune the thermoelectric prop-

erty. This work may have potential applications in graphene-based heterostructures devices.

This project was supported by the National Science Foundation of China (Grant Nos. 10834011, 60620120443, and 60621061), the National "973" projects of China (Grant Nos. 2006CB921305 and 2009CB929103), and DOE-BES of United States of American.

<sup>1</sup>K. S. Novoselov, Z. Jiang, Y. Zhang, S. V. Morozov, H. L. Stormer, U. Zeitler, J. C. Maan, G. S. Boebinger, P. Kim, and A. K. Geim, *Science* **315**, 1379 (2007).

<sup>2</sup>K. S. Novoselov, A. K. Geim, S. V. Morozov, D. Jiang, M. I. Katsnelson, I. V. Grigorieva, S. V. Dubonos, and A. A. Firsov, *Nature (London)* **438**, 197 (2005).

<sup>3</sup>N. Tombros, C. Jozsa, M. Popinciuc, H. T. Jonkman, and B. J. van Wees, *Nature (London)* **448**, 571 (2007).

<sup>4</sup>J. S. Bunch, A. M. van der Zande, S. S. Verbridge, I. W. Frank, D. M. Tanenbaum, J. M. Parpia, H. G. Craighead, and P. L. McEuen, *Science* **315**, 490 (2007).

<sup>5</sup>D. A. Abanin and L. S. Levitov, *Science* **317**, 641 (2007).

<sup>6</sup>V. V. Cheianov, V. Fal'ko, and B. L. Altshuler, *Science* **315**, 1252 (2007).

<sup>7</sup>J. R. Williams, L. DiCarlo, and C. M. Marcus, *Science* **317**, 638 (2007).

<sup>8</sup>Q. M. Yan, B. Huang, J. Yu, F. W. Zheng, J. Zang, J. Wu, B. L. Gu, F. Liu, and W. H. Duan, *Nano Lett.* **7**, 1469 (2007).

<sup>9</sup>C. Berger, Z. M. Song, X. B. Li, X. S. Wu, N. Brown, C. Naud, D. Mayo, T. B. Li, J. Hass, A. N. Marchenkov, E. H. Conrad, P. N. First, and W. A. de Heer, *Science* **312**, 1191 (2006).

<sup>10</sup>S. Marchini, S. Gunther, and J. Wintterlin, *Phys. Rev. B* **76**, 075429 (2007).

<sup>11</sup>A. L. Vázquez de Parga, F. Calleja, B. Borca, M. C. G. Passeggi, J. J. Hinarejos, F. Guinea, and R. Miranda, *Phys. Rev. Lett.* **100**, 056807 (2008).

<sup>12</sup>Y. Pan, H. Zhang, D. Shi, J. Sun, S. Du, F. Liu, and H. Gao, *Adv. Mater.* **21**, 2777 (2009).

<sup>13</sup>A. T. N'Diaye, J. Coraux, T. N. Plasa, C. Busse, and T. Michely, *New J. Phys.* **10**, 043033 (2008).

<sup>14</sup>C. A. Di, D. C. Wei, G. Yu, Y. Q. Liu, Y. L. Guo, and D. B. Zhu, *Adv. Mater.* **20**, 3289 (2008).

<sup>15</sup>K. J. Kim, H. Lee, J. H. Choi, Y. S. Youn, J. Choi, H. Lee, T. H. Kang, M. C. Jung, H. J. Shin, H. J. Lee, S. Kim, and B. Kim, *Adv. Mater.* **20**, 3589 (2008).

<sup>16</sup>M. Enachescu, D. Schleef, D. F. Ogletree, and M. Salmeron, *Phys. Rev. B* **60**, 16913 (1999).

<sup>17</sup>Note that we used a 30° rotational angle in DFT calculation different from the 14° angle seen in the experiment. This is because constructing a 14° rotated graphene domain superstructure on Pt(111) would require too large a supercell, beyond the present-day capability of DFT calculations.

<sup>18</sup>X. Lin, X. B. He, J. L. Lu, L. Gao, Q. Huan, D. X. Shi, and H. J. Gao, *Chin. Phys.* **14**, 1536 (2005).

<sup>19</sup>D. Dragoman and M. Dragoman, *Appl. Phys. Lett.* **91**, 203116 (2007).

<sup>20</sup>H. Hu, J. M. Cai, C. D. Zhang, M. Gao, Y. Pan, S. X. Du, Q. F. Sun, Q. Liu, X. C. Xie, and H. J. Gao, *Chin. Phys. B* 2010 (accepted).

<sup>21</sup>G. Bertoni, L. Calmels, A. Altibelli, and V. Serin, *Phys. Rev. B* **71**, 075402 (2005).

<sup>22</sup>K. Yamamoto, M. Fukushima, T. Osaka, and C. Oshima, *Phys. Rev. B* **45**, 11358 (1992).